CONF-950961--3

PNL-SA-24375



# MICROSTRUCTURAL EXAMINATION OF COMMERCIAL FERRITIC ALLOYS AT 200 DPA

D.S. Gelles

November 1995

Presented at the
Fusion Reactor Materials 7th International Conference
Fall 1995
Russia

Work supported by
the U.S. Department of Energy
under Contract DE-AC06-76RLO 1830

Pacific Northwest Laboratory
Richland, WA 99352

# MICROSTRUCTURAL EXAMINATION OF COMMERCIAL FERRITIC ALLOYS AT 200 DPA -

D. S. Gelles, (Pacific Northwest Laboratory)[a]

## OBJECTIVE

The objective of this work is to determine lifetime limits for ferritic/Martensitic alloys.

## SUMMARY

Microstructures and density change measurements are reported for Martensitic commercial steels HT-9 and Modified 9Cr-1Mo (T9) and oxide dispersion strengthened ferritic alloys MA956 and MA957 following irradiation in the FFTF/MOTA at 420°C to 200 DPA. Swelling as determined by density change remains below 2% for all conditions. Microstructures are found to be stable except in recrystallized grains of MA957, which are fabrication artifacts, with only minor swelling in the Martensitic steels and $\alpha'$ precipitation in alloys with 12% or more chromium. These results further demonstrate the high swelling resistance and microstructural stability of the ferritic alloy class.

## PROGRESS AND STATUS

### Introduction

Reduced activation ferritic alloys appear to be promising first wall and structural materials for commercial fusion reactors. This expectation is based in part on limited experiments using reduced activation alloys, but also on a large number of experiments using commercial ferritic/Martensitic alloys. The present effort investigates the high dose limit of the commercial steels by examining the effect of irradiation in a fast reactor at the peak swelling temperature to a very high dose, not likely to be exceeded for many years.

The materials being examined include two classes, Martensitic stainless steels in the 9 to 12% Cr range and oxide dispersion strengthened (ODS) alloys made by the mechanical alloying process. The Martensitic steels are HT-9 and Modified 9Cr-1Mo (now designated as T9), and the ODS alloys are MA956 and MA957. The original candidate ferritic alloy for fusion structural materials applications was HT-9, an Fe-12Cr-1Mo-0.2C-WV steel. Due to better irradiation embrittlement expectations, T9, an Fe-9Cr-1Mo-0.1C-VNb steel, was considered an alternative to HT-9. Mechanical alloying, a process using high energy ball milling procedures, is expected to provide a ferritic alloy option with applications to significantly higher temperatures,[1,2] albeit with worst ductile to brittle transition temperature response. The first ferritic alloy to be manufactured commercially using mechanical alloying was MA956, an Fe-20Cr-4Al-0.5Ti-0.5$Y_2O_3$. A similar alloy with lower chromium, MA957, was invented for radiation damage resistance.[3] It may be noted that results of microstructural examination have been reported previously for identical specimens of HT-9 to the lower dose of 110 dpa,[4] and the density measurements for HT-9 and T9 at 200 dpa have already been reported.[5] The International Nickel Company kindly provided the two experimental batches of MA957 for irradiation before commercial production was available.

---

[a]Pacific Northwest Laboratory is operated for the U.S. Department of Energy by Battelle Memorial Institute under Contract DE-AC06-76RLO 1830.

DOE/ER-0313/14

# MICROSTRUCTURAL EXAMINATION OF COMMERCIAL FERRITIC ALLOYS AT 200 DPA

D. S. Gelles, (Pacific Northwest Laboratory)*

## OBJECTIVE

The objective of this work is to determine lifetime limits for ferritic/Martensitic alloys.

## SUMMARY

Microstructures and density change measurements are reported for Martensitic commercial steels HT-9 and Modified 9Cr-1Mo (T9) and oxide dispersion strengthened ferritic alloys MA956 and MA957 following irradiation in the FFTF/MOTA at 420°C to 200 DPA. Swelling as determined by density change remains below 2% for all conditions. Microstructures are found to be stable except in recrystallized grains of MA957, which are fabrication artifacts, with only minor swelling in the Martensitic steels and α' precipitation in alloys with 12% or more chromium. These results further demonstrate the high swelling resistance and microstructural stability of the ferritic alloy class.

## PROGRESS AND STATUS

### Introduction

Reduced activation ferritic alloys appear to be promising first wall and structural materials for commercial fusion reactors. This expectation is based in part on limited experiments using reduced activation alloys, but also on a large number of experiments using commercial ferritic/Martensitic alloys. The present effort investigates the high dose limit of the commercial steels by examining the effect of irradiation in a fast reactor at the peak swelling temperature to a very high dose, not likely to be exceeded for many years.

The materials being examined include two classes, Martensitic stainless steels in the 9 to 12% Cr range and oxide dispersion strengthened (ODS) alloys made by the mechanical alloying process. The Martensitic steels are HT-9 and Modified 9Cr-1Mo (now designated as T9), and the ODS alloys are MA956 and MA957. The original candidate ferritic alloy for fusion structural materials applications was HT-9, an Fe-12Cr-1Mo-0.2C-WV steel. Due to better irradiation embrittlement expectations, T9, an Fe-9Cr-1Mo-0.1C-VNb steel, was considered an alternative to HT-9. Mechanical alloying, a process using high energy ball milling procedures, is expected to provide a ferritic alloy option with applications to significantly higher temperatures,[1,2] albeit with worst ductile to brittle transition temperature response. The first ferritic alloy to be manufactured commercially using mechanical alloying was MA956, an Fe-20Cr-4Al-0.5Ti-0.5$Y_2O_3$. A similar alloy with lower chromium, MA957, was invented for radiation damage resistance.[3] It may be noted that results of microstructural examination have been reported previously for identical specimens of HT-9 to the lower dose of 110 dpa,[4] and the density measurements for HT-9 and T9 at 200 dpa have already been reported.[5] The International Nickel Company kindly provided the two experimental batches of MA957 for irradiation before commercial production was available.

---

*Pacific Northwest Laboratory is operated for the U.S. Department of Energy by Battelle Memorial Institute under Contract DE-AC06-76RLO 1830.

The present experiment is based on specimens included in early Fast Flux Test Facility/Materials Open Test Assembly (FFTF/MOTA) irradiation tests. The tests were continued until the shutdown of the reactor. Specimens were in weeper positions operating at temperatures on the order of 420°C, the temperature range found to result in peak swelling for the ferritic alloy class. As a result, examination of these specimens allows the opportunity to evaluate the ferritic alloy class at extremely high dose, in order to assess life limiting conditions for Martensitic and ODS steels.

## Experimental Procedure

The alloy compositions and heat treatments are provided in Table 1. As indicated in the identification (ID) codes, specimens of HT-9 and T9 were included in transmission electron microscopy (TEM) packet FL whereas specimens of MA956 and MA957 were in TEM packet H4. TEM packets FL and H4 were located in in-core weeper positions of the FFTF/MOTA from the beginning of cycle 4 and throughout the operation of FFTF. The irradiation history for packet FL was as follows:

MOTA 1B basket 1E-4 to $2.21 \times 10^{22}$ n/cm$^2$ (all fluences are given as E > 0.1 MeV) at an average temperature of 407°C.
MOTA 1C basket 2C-4 to $7.25 \times 10^{22}$ n/cm$^2$ at 425°C.
MOTA 1D basket 2C-2 to $5.46 \times 10^{22}$ n/cm$^2$ at 406°C.
MOTA 1E basket 2C-2 to $9.59 \times 10^{22}$ n/cm$^2$ at 403°C.
MOTA 1F basket 2C-1 to $9.58 \times 10^{22}$ n/cm$^2$ at 406°C.
MOTA 1G basket 3A-1 to $7.96 \times 10^{22}$ n/cm$^2$ at 431°C.
MOTA 2B basket 3A-4 to $6.38 \times 10^{22}$ n/cm$^2$ at 433°C.

Table 1. Compositions of commercial ferritic/Martensitic alloys

| ID Code | Alloy | Heat No. | Composition (w/o) | | | | | | | | | | HT* |
|---|---|---|---|---|---|---|---|---|---|---|---|---|---|
| | | | Cr | C | Mo | V | Mn | Si | Ni | P | S | Other | |
| PTFL | T9 | 30176 | 8.43 | .09 | .89 | .24 | .37 | .16 | .11 | .011 | .004 | Nb: .08<br>Cu: .04 | A |
| RFFL<br>RHFL | HT-9 | 9607R2 | 12.1 | .20 | 1.04 | 0.28 | 0.57 | .17 | .51 | .016 | .003 | N: .027<br>W: .45 | B<br>C |
| RLH4 | MA956 | ABB0042 | 19.10 | .019 | na | na | 0.09 | .10 | .19 | .009 | .004 | $Y_2O_3$: .48<br>Al: 4.20<br>Ti: .34 | D |
| RMH4 | MA957 | T88793 | 13.8 | na | 0.26 | na | na | na | na | na | na | $Y_2O_3$: .26<br>Ti: .90<br>O(total): .32<br>N: .031 | E |
| RNH4 | MA957 | T88794 | 13.1 | na | 0.27 | na | na | na | na | na | na | $Y_2O_3$: .25<br>Ti: .95<br>O(total): .28<br>N: .036 | E |

* HEAT TREATMENTS with AC = air cooled, RT = room temperature
A = 1040°C/1 hr/AC to RT + 760/1 hr/AC
B = 1000°C/20 hr/AC to RT + 1100/5 min/AC to RT + 700/2 hr/AC
C = 1050/5 min/AC to RT + 760/0.5 hr/AC
D = 1330°C/1 hr/AC
E = 1100°C/1 hr/AC

Therefore, during that period, the specimens in packet FL received a fluence of $4.84 \times 10^{23}$ n/cm$^2$ at an average temperature of 416 ± 13°C, hereafter reported as 420°C. The irradiation history for packet H4 was as follows:

MOTA 1B basket 2F-5 to $2.98 \times 10^{22}$ n/cm$^2$ at an average temperature of 431°C.
MOTA 1C basket 2F-5 to $6.98 \times 10^{22}$ n/cm$^2$ at 420°C.
MOTA 1D basket 2F-5 to $5.05 \times 10^{22}$ n/cm$^2$ at 404°C.
MOTA 1E basket 2F-2 to $9.67 \times 10^{22}$ n/cm$^2$ at 414°C.
MOTA 1F basket 2F-2 to $9.60 \times 10^{22}$ n/cm$^2$ at 405°C.
MOTA 1G basket 2E-3 to $7.18 \times 10^{22}$ n/cm$^2$ at 417°C.
MOTA 2B basket 3A-5 to $6.35 \times 10^{22}$ n/cm$^2$ at 433°C.

Therefore, during that period, the specimens in packet H4 received a fluence of $4.78 \times 10^{23}$ n/cm$^2$ at an average temperature of 418 ± 11°C, hereafter reported as 420°C. The dose achieved, calculated from reference[6] which is based on dosimetry measurements from MOTA 1F, varies from 200 to 202 dpa, depending on alloy composition.

Microstructural examinations were performed on a JEOL JEM 1200EX scanning TEM operating at 120 kV and outfitted with a Tracor Northern energy dispersive x-ray fluorescence (EDX) detector and TN5500 computer and with a Gatan Electron energy loss spectrometer. Determination of precipitate compositions from extraction replicas involved computer analysis of EDX spectra which included analysis for tungsten.

## Results

### Swelling

Results of density change measurements for commercial alloy specimens irradiated at 420°C to 200 dpa are provided in Table 2. Table 2 contains dose estimates for each alloy based on conversions from reference.[6] As shown from Table 2, swelling values are in the range 0.09 to 1.76%. The highest swelling values are for T9 and one of the heats of MA957. All others are at about 1% or less. Therefore, commercial ferritic steels are extremely resistant to radiation induced void swelling.

Table 2. Swelling as measured by density change for commercial ferritic/Martensitic alloy specimens.

| CODE | Alloy | Heat Treatment | Dose (dpa) | Density Irradiated | Density Unirradiated | Swelling (%) |
|---|---|---|---|---|---|---|
| PTFL | T9 | 760/1 hr/AC | 201.4 | 7.65245 | 7.7869 | 1.76 |
| RFFL | HT-9 | 700/2 hr/AC | 201.6 | 7.78535 | 7.7924 | 0.09 |
| RHFL | HT-9 | 760/0.5 hr/AC | 201.6 | 7.76079 | 7.84079 | 1.02 |
| RLH4 | MA956 | 1330°C/1 hr/AC | 201.3 | 7.27343 | 7.35823 | 1.17 |
| RMH4 | MA957 | 1100°C/1 hr/AC | 200.0 | 7.61565 | 7.74904 | 1.75 |
| RNH4 | MA957 | 1100°C/1 hr/AC | 199.9 | 7.64425 | 7.66355 | 0.25 |

However, significant variation can exist between different heats or different heat treatments of the same steel. Both in the case of MA957 where two different batches of materials are compared, and

HT-9 where the same steel in two different heat treatments is compared, swelling varies between less than 0.25% and over 1%.

Microstructural examination

Microstructural examinations revealed that following irradiation at 420°C to 200 dpa, all specimens contained cavities, typical of void swelling. However, large regions in each of the MA957 specimens contained negligible cavitation, and the cavitation present in those regions is expected to be a remnant of the mechanical alloying process. In contrast, there were regions in the MA957 specimens where significant void swelling and dislocation evolution had developed. The T9 and HT-9 conditions developed void structures typical of martensitic steels. These void structures consisted of void arrays between lath boundaries and void free regions on, and adjacent to, the boundaries.

Low magnification examples are provided in Figure 1. Figure 1 shows Martensite lath boundary structures in irradiated T9 and HT-9, and subgrain structures selected to show the most typical regions for irradiated MA956 and MA957. The example for T9 in Figure 1a is found to contain a fairly uniform array of voids within laths and a moderate density of blocky carbide precipitate decorating subgrain boundaries. Figures 1b and 1c for HT-9 show structures with significantly more blocky precipitation decorating boundaries and a lower density of sightly larger voids. It may also be noted that the foil shown in Figure 1c was attacked non-uniformly by the electropolishing electrolyte, indicating that some large scale compositional variation may develop at high dose. Figure 1d provides an example of MA956 that shows a uniform structure, containing voids but with several very large precipitate particles and a typical wavy grain boundary. No evidence of subgrain structure was found in this material. Figures 1e and 1f provide examples of the fine subgrain structure retained in MA957. Cavitation in these subgrains is very limited. However, precipitation can be noted throughout. The precipitation is expected to include both yttria and $\alpha'$, a body centered cubic phase rich in chromium. Many examples can be found where subgrain boundaries are denuded of precipitation. The denuded regions are typically about 15 nm wide. Also, it should be noted that Figure 1f has been selected to show a region at the lower right containing a well developed array of voids. Further discussion of these features will follow.

Figure 2 provides examples (at higher magnification) of the microstructure found in T9 following irradiation at 420°C to 200 dpa. Figures 2a, 2b, and 2c provide different imaging conditions for the same region to define the dislocation structures. Figures 2a and 2b use $\vec{g} = 200$ and $1\bar{1}0$ respectively for an (001) foil orientation, and Figure 2c provides a view of the voids in absorption contrast. By comparing Figures 2a and 2b, it can be shown that the dislocation structure is comprised of a<100> loops and a network of $\frac{a}{2}$<111> dislocation segments. Figure 2d gives another example of $\vec{g} = 1\bar{1}0$ contrast for a foil near ($\bar{0}01$) with similar dislocation development. However, Figures 2e and 2f show a third region in $\vec{g} = 200$ and $01\bar{1}$ contrast for an (011) foil. In this case, the dislocation structure is predominantly of Burgers vector $\frac{a}{2}$<111>. This difference may be a result of the nearby subgrain boundaries, which provided dislocation sources. However, the void structure appears similar in all three areas, indicating that Burgers vector variations have only small effects on void evolution.

Figure 3 provides examples at higher magnification of the microstructures found in irradiated HT-9 following a 700°C temper. The microstructures are typical of HT-9 irradiated at 420°C, and show well developed precipitate arrays decorating subgrain lath boundaries, non-uniform void arrays within laths and a fine precipitate on boundaries and within laths. An area is shown in dislocation, void and precipitate contrast, Figures 3a and 3b in $\vec{g} = 200$ and $01\bar{1}$ contrast, Figure 3c in void contrast, and Figure 3d in $\vec{g} = \frac{1}{3}[333]$ for a foil near 011. From these figures,

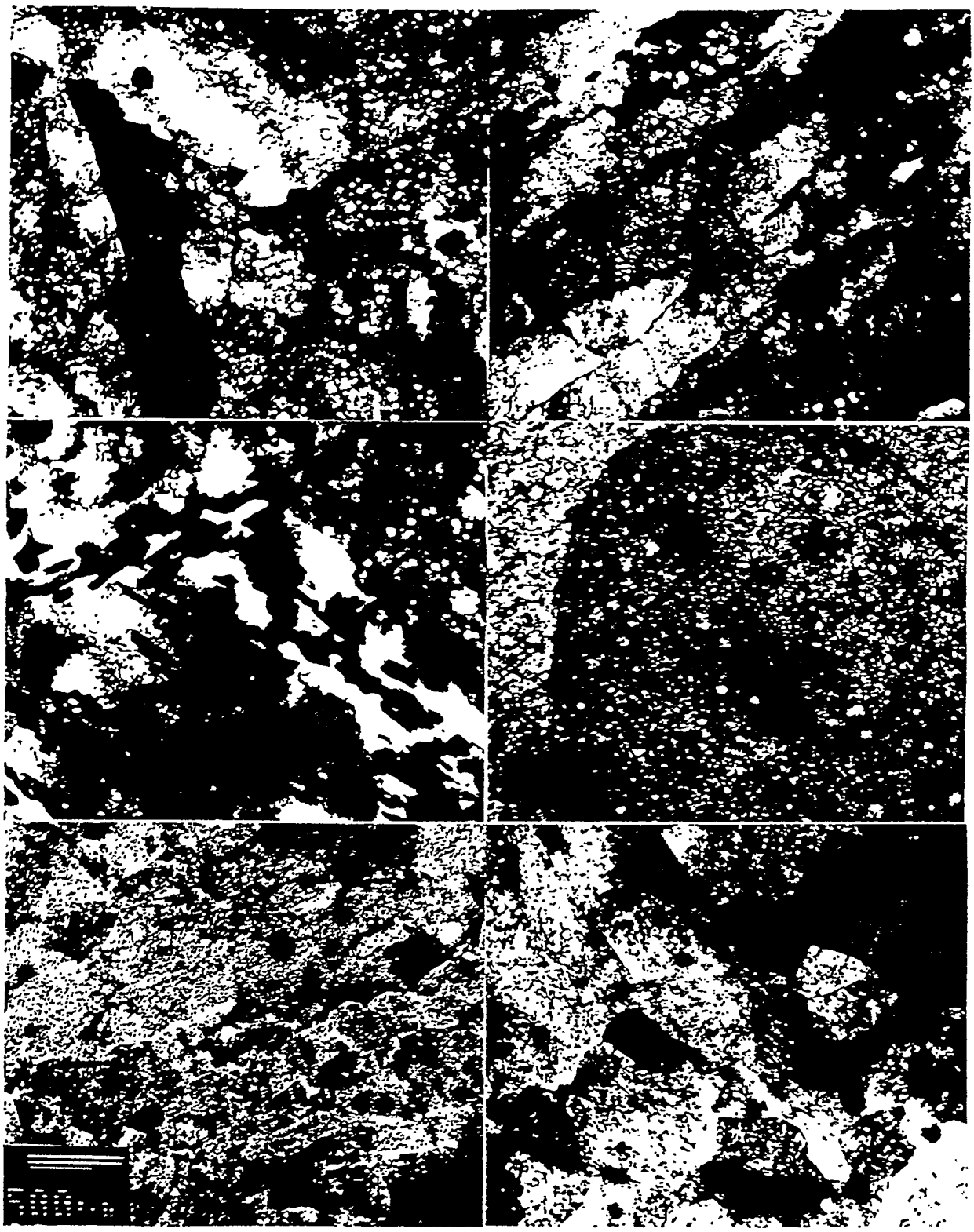

Figure 1. Microstructures at low magnification of Commercial Ferritic Alloys Following Irradiation at 420°C to 200 dpa (a) T9, (b) HT-9 heat treated at 700°C, (c) HT-9 heat treated at 760°C, (d) MA956, (e) MA957 heat T88793 and (f) MA957 heat T88794.

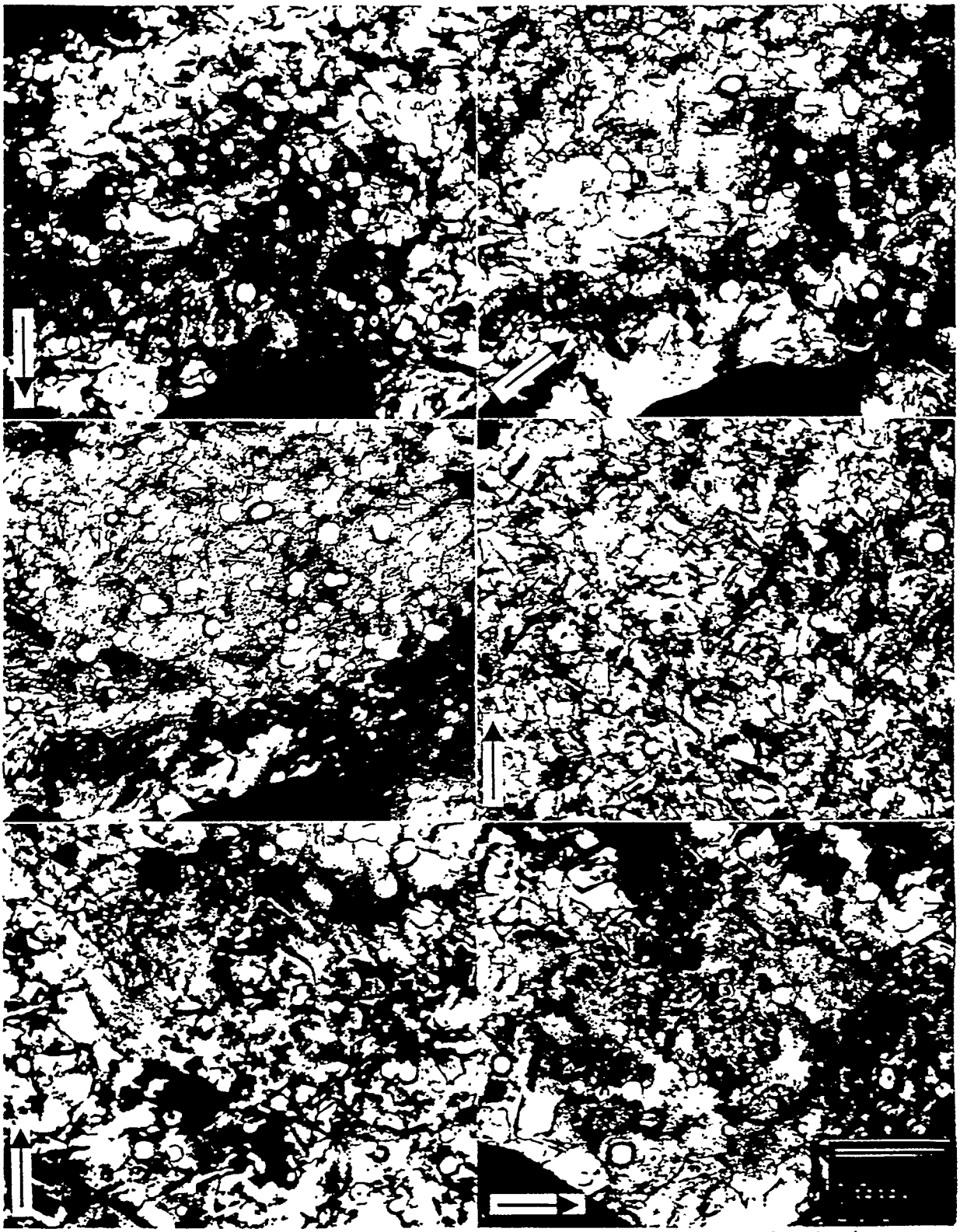

Figure 2. Dislocation and Void Microstructures for T9 irradiated at 420°C to 200 dpa showing an (001) foil orientation in a) 200 contrast, and b) $1\bar{1}0$ contrast, c) a second area in $1\bar{1}0$ contrast and a third area in an (011) foil orientation in d) 200 contrast, e) $01\bar{1}$ contrast and f) void contrast.

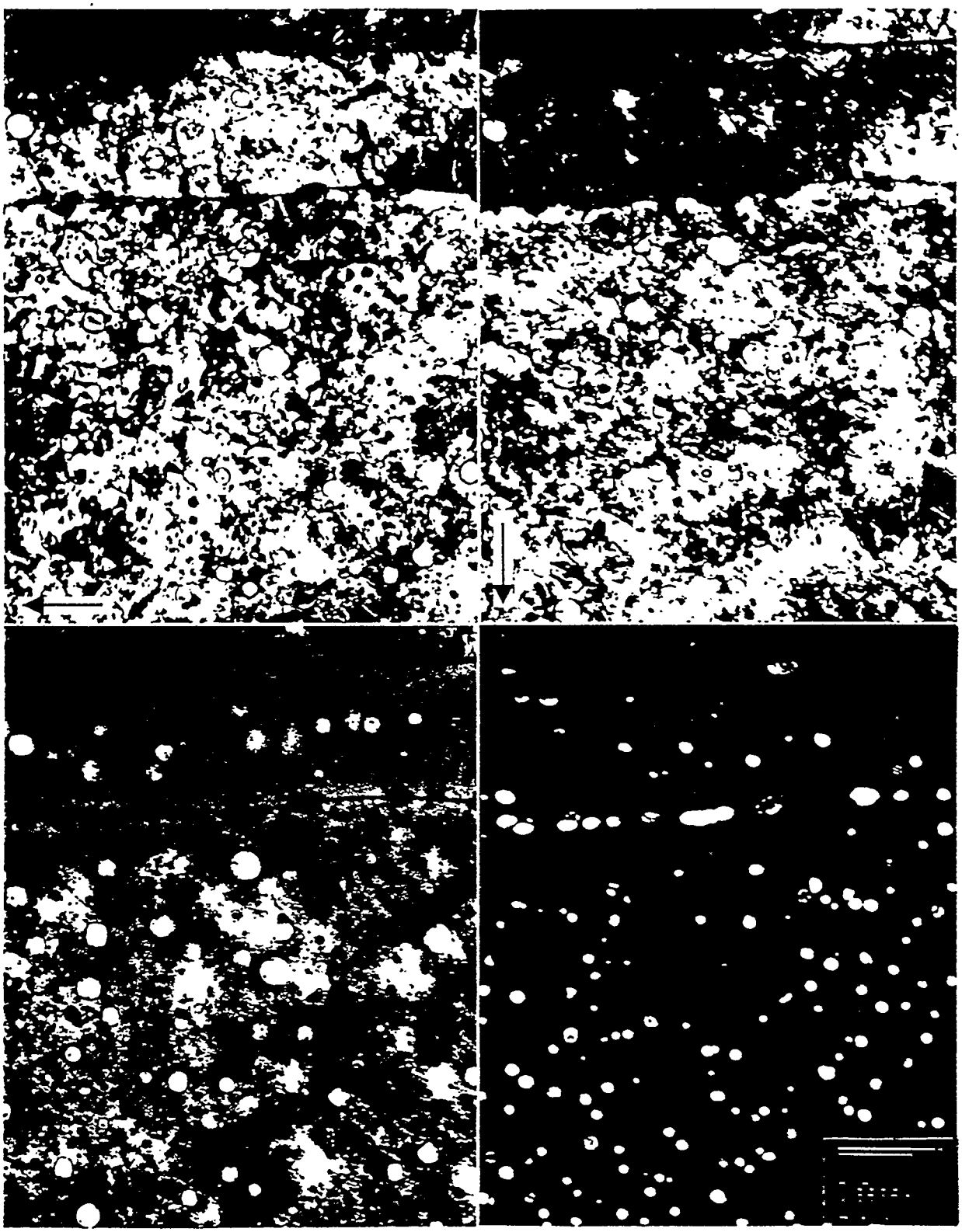

Figure 3. Microstructures of HT-9 tempered at 700°C and irradiated at 420°C to 200 dpa showing an (011) foil orientation in a) 200 contrast, b) $01\bar{1}$ contrast, c) void contrast and d) dark field precipitate contrast.

it can be shown that the dislocation structure is predominantly of type $\frac{a}{2}$<111>, but with a low density of a<100> loops, and that voids vary in shape between cubes with {011} truncation and even truncation between cubes and dodecahedra. Figure 3d is intended to show the precipitation that is found in irradiated HT-9 and has previously been called G-phase by the author. The precipitate is 10 nm in diameter within laths, but somewhat larger on subgrain boundaries. Irradiation hardening found in HT-9 can be attributed to this phase. However, comparison of Figures 3c and 3d reveals that not all precipitates are imaged in Figure 3d; the smaller ones do not appear. These smaller precipitates are expected to be α'.

Figure 4 provides similar examples for irradiated HT-9 following a temper at 760°C. Two areas are shown in dislocation and void contrast, Figures 4a and 4e in $\vec{g}$ = 200 contrast, Figures 4b and 4f in $01\bar{1}$ contrast, and Figures 4c and 4d in void contrast for foils near (001) and (011) orientations, respectively. From these figures, it can be shown that dislocation structures contain both a<100> loops and $\frac{a}{2}$<111> network segments, but where subgrain boundaries are present, the a<100> dislocation density is significantly reduced. Also, voids vary in shape, but are generally evenly truncated between cubes and dodecahedra. Evidence for the fine precipitate noted in Figure 3 can be found.

Figure 5 provides an example of the microstructures found in MA956 following irradiation at 420°C to 200 dpa. The same region is imaged in $\vec{g}$ = 200, $01\bar{1}$, and absorption contrast (to show voids) for a foil near an (011) orientation. The dislocation images are difficult to interpret, but the presence of both a<100> loops and $\frac{a}{2}$<111> network segments can be identified. The voids in Figure 5c are found to vary in shape, but the dominant configuration is cuboidal with (111) octahedral facets. Comparison with other void images in this report will confirm that the voids in MA956 are different, showing clear (111) facets. Figure 5c also reveals the presence of precipitation, typical of α', as expected for an alloy with 19% Cr. The complex dislocation imaging and variability in void shape are likely due to the α' formation. However, it is noteworthy that again, no evidence of subgrain structure can be identified.

Figures 6 and 7 give examples of the microstructures found in the experimental batches of MA957 following irradiation at 420°C to 200 dpa. Figure 6 shows three areas in batch T88793 with varying levels of void swelling. Figure 6a gives an example where no voids are present; only a mottled background due to precipitation can be seen. The precipitation is expected to include both α' and yttria ($Y_2O_3$), and based on experience imaging the yttria in unirradiated MA957 where particle diameters are about 2 nm, the precipitation apparent in Figure 6a is expected to be α'. Figure 6b shows an area containing two subgrains that have developed voids on the order of 40 nm in diameter. One of the void arrays is linear, indicating that void nucleation was heterogeneous. Figures 6c and 6d show an area in an (011) orientation using 200 and $01\bar{1}$ contrast, respectively. Comparing these images indicates that a few a<100> loops are present, but the dislocation structure is comprised mainly of $\frac{a}{2}$<111> dislocation segments (and α' precipitates complicate the analysis). Voids are generally evenly truncated between cubic and dodahedral shapes. Figure 7 provides a similar comparison for a large grain near (011) orientation, with adjacent subgrains that contain no voids. Figures 7a and 7b show dislocation imaging in the large grain using $\vec{g}$ = 200 and $01\bar{1}$, respectively, and Figure 7c provides void contrast. From this sequence, similar observations can be made: the dislocation structure consists predominantly of $\frac{a}{2}$<111> dislocation segments, and voids are evenly truncated between cubic and dodecahedral geometries.

A summary of microstructural observations is tabulated in Table 3. From Table 3, it can be shown that the swelling was measured as high as 5% in isolated regions, that the dislocation structure contains both $\frac{a}{2}$<111> and a<100> Burgers vectors, and voids are generally truncated

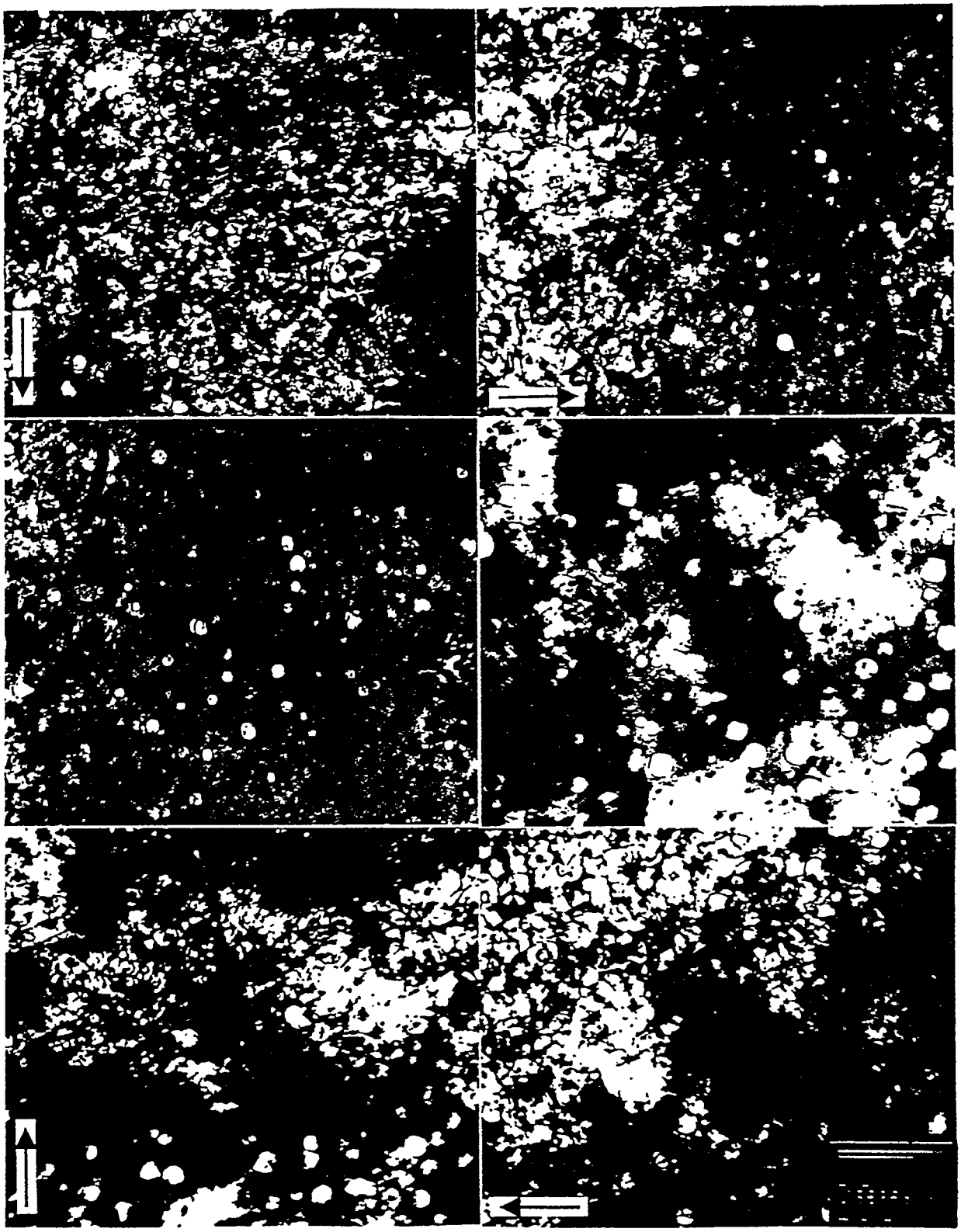

Figure 4. Dislocation and Void Microstructures for HT-9 tempered at 760°C and irradiated at 420°C to 200 dpa showing (011) foil orientations for two areas in a) and e) 200 contrast, b) and f) $01\bar{1}$ contrast and c) and d) void contrast, respectively.

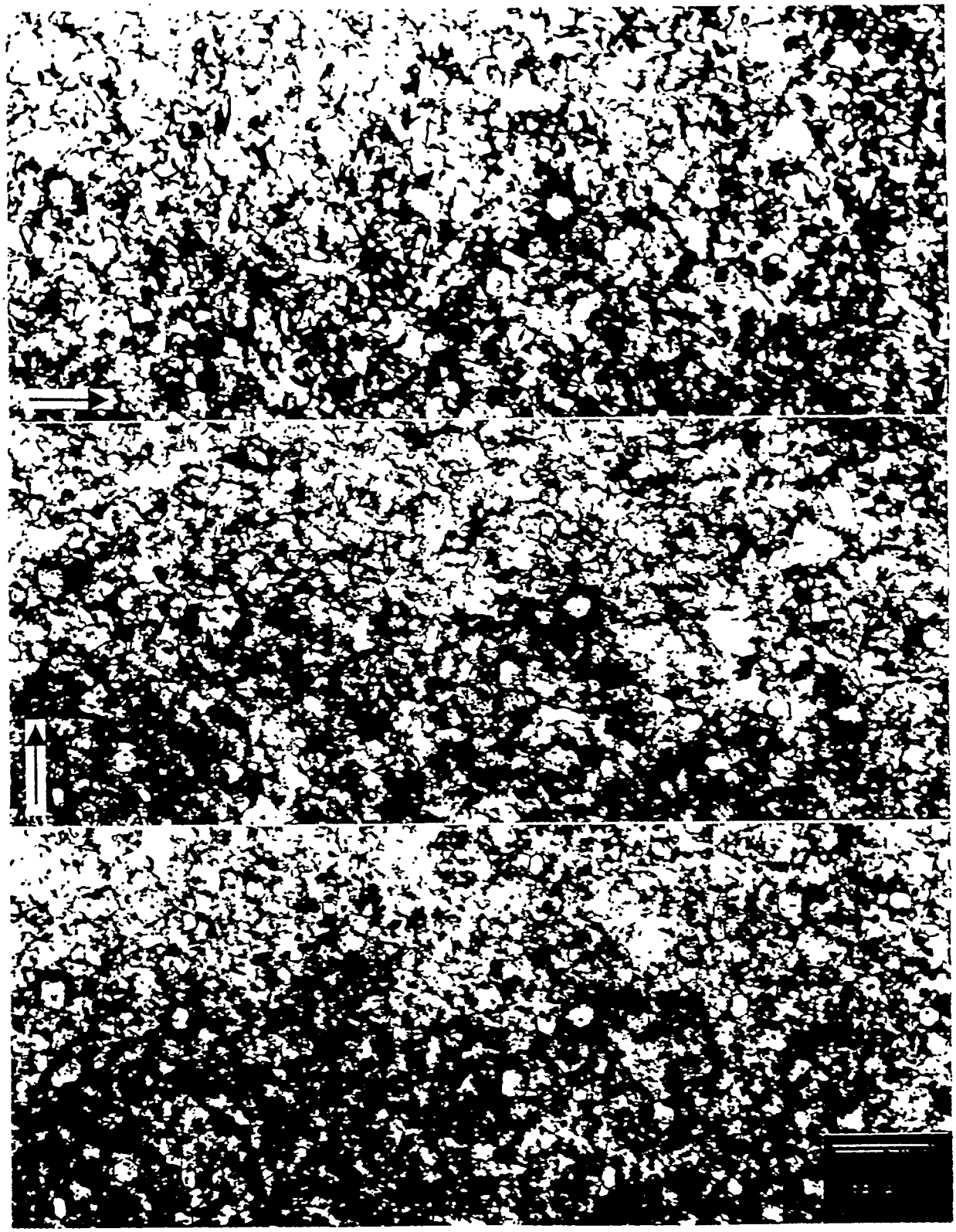

Figure 5. Example of the Microstructures found in MA956 following irradiation at 420°C to 200 dpa showing a region with foil orientation (011) in a) 200 contrast, b) in $01\bar{1}$ contrast, and c) in void contrast.

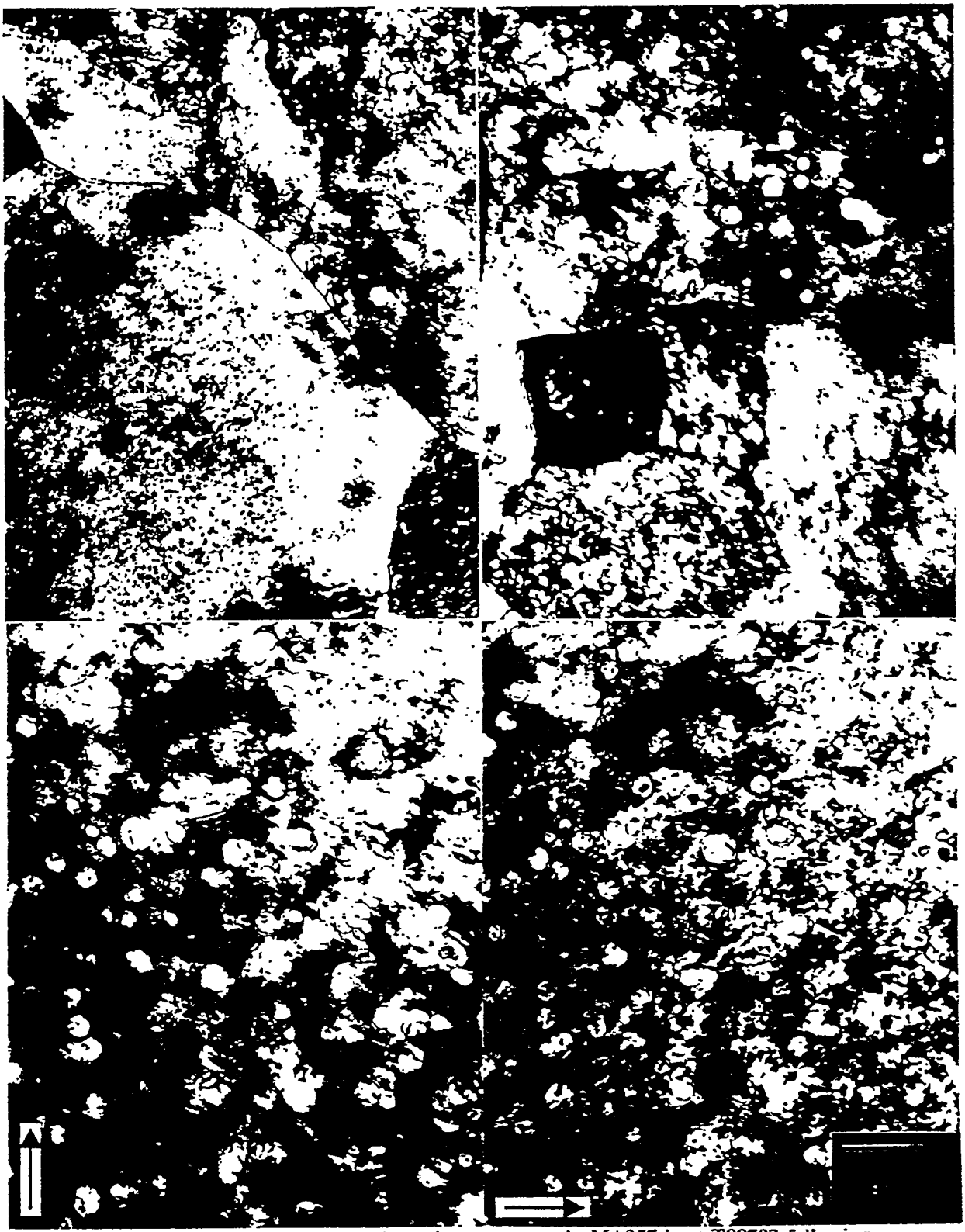

Figure 6. Precipitate, void and dislocation microstructures in MA957 heat T88793 following irradiation at 420°C to 200 dpa for a) a region containing no voids, b) a region containing a moderate void density and for a region in (011) orientation containing a well developed void array in c) 200 contrast and d) 011 contrast.

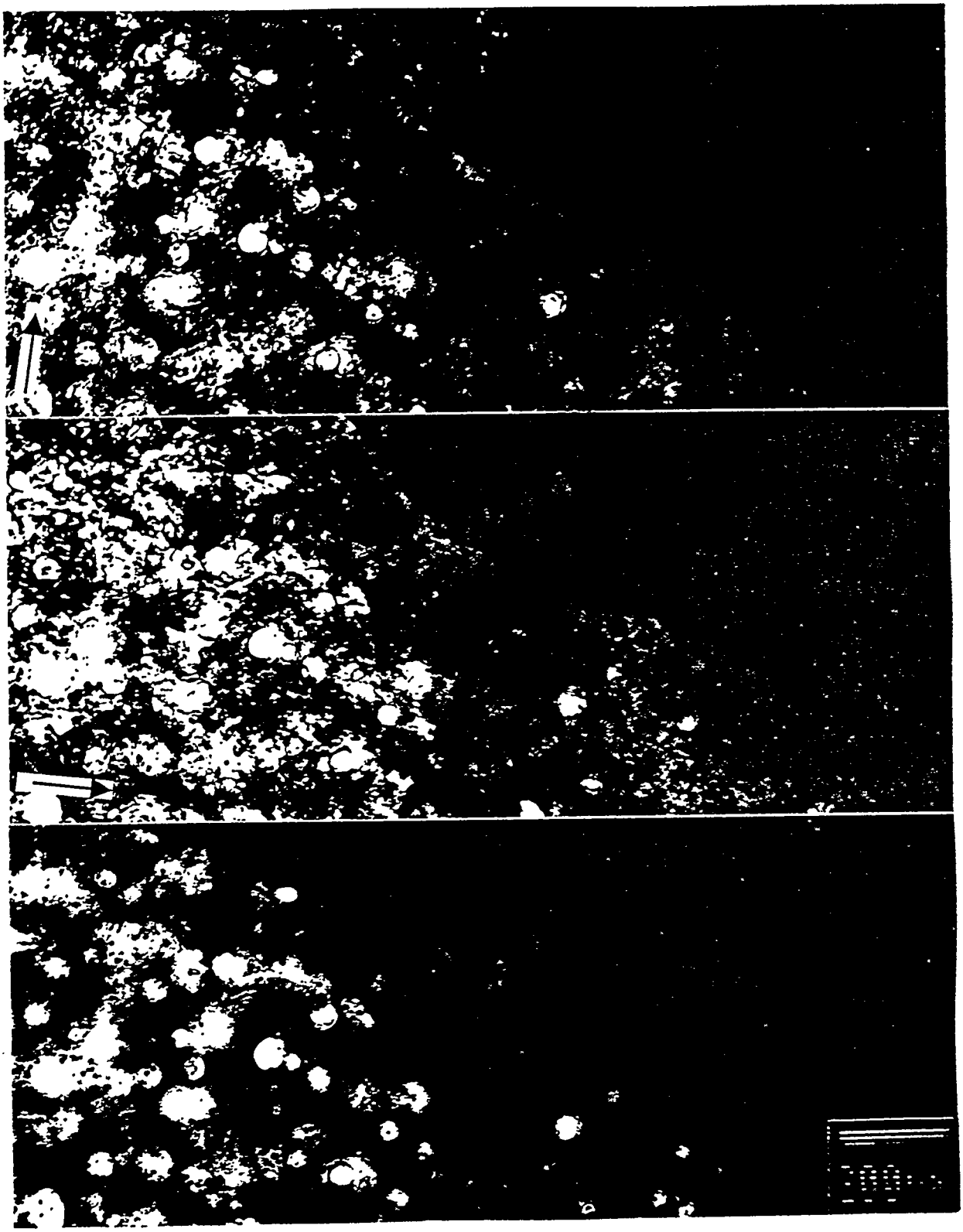

Figure 7. Microstructures in MA957 heat T88794 following irradiation at 420°C to 200 dpa for a grain containing voids in (011) orientation in a) 200 contrast, b) $01\bar{1}$ contrast and c) void contrast.

between dodecahedra and cubes. The void truncation notation is intended to mean that the (100) and (110) facets are about equal in size.

Discussion

The results of this work are highly encouraging. Commercial ferritic/Martensitic alloys are demonstrated to have the high dose swelling resistance and microstructural stability that had been predicted.[7] Although precipitate identification is incomplete, the phases present seem to match those found at lower dose. The Martensite lath structure is also retained. Swelling is found in both Martensitic stainless steels, but the levels of swelling are very modest, and the swelling is not expected to alter mechanical properties significantly. Blocky precipitation on prior austenite and subgrain boundaries is enhanced compared to the preirradiation condition, and some degradation of properties can be envisioned, such as Charpy impact. Also, in a fusion

Table 3. Summary of microstructural observations.

| CODE | Alloy | Dose (dpa) | Highest Swelling (%) | Mean Void Size (nm) | Void Density ($\#/cm^3$) | Void Shape | Dislocation Structure |
|---|---|---|---|---|---|---|---|
| PTFL | T9 | 203.2 | 5.0 | 21.4 | $4.8 \times 10^{15}$ | truncated between dodecahedra and cubes | examples of both primarily $\frac{a}{2}$<111> network and primarily a<100> network |
| RFFL | HT-9 | 203.5 | 3.2 | 21.2 | $3.1 \times 10^{15}$ | truncated dodecahedra | a<100> loops and primarily $\frac{a}{2}$<111> network |
| RHFL | HT-9 | 204.0 | 1.7 | 32.2 | $5.6 \times 10^{14}$ | truncated between cubes and dodecahedra | a<100> loops and primarily $\frac{a}{2}$<111> network |
| RLH4 | MA956 | 204.8 | 0.21 | 26.7 | $1.9 \times 10^{14}$ | truncated between cubes and octahedra | a<100> loops and primarily $\frac{a}{2}$<111> network |
| RMH4 | MA957 | 205.7 | 3.7 | 36.1 | $9.2 \times 10^{14}$ | truncated between dodecahedra and cubes | original ODS structure retained, a<100> & $\frac{a}{2}$<111> loops and $\frac{a}{2}$<111> network in recrystallized regions |
| RNH4 | MA957 | 206.0 | 3.5 | 35.4 | $8.6 \times 10^{14}$ | truncated between dodecahedra and cubes | original ODS structure retained, a<100> & $\frac{a}{2}$<111> loops and $\frac{a}{2}$<111> network in recrystallized regions |

environment, transmutation of iron to manganese will encourage further FeCrMn chi phase development. Therefore, intermetallic precipitation is expected to be the metallurgical process controlling properties and life limits at high dose.

Results of radiation damage resistance of ODS ferritic alloys are even more encouraging. Evidence was apparent in both MA956 and MA957 for $\alpha'$ precipitation, and in regions where recrystallization had occurred before irradiation in MA957, void development was extensive. But both these problems can be overcome by suitable alloy design. The ODS alloy microstructures, when properly manufactured to provide a uniform oxide dispersoid in a subgrain structure, appear to be completely radiation damage resistant to doses as high as 200 dpa.

Other observations are worthy of further emphasis. Regions were found in both Martensitic alloys where comparable void development had occurred, but the dislocation structures were quite different. Apparently, void swelling is unaffected by whether the dislocation structure contains a significant a<100> component. Possible explanations for low swelling in ferritic alloys were based on the presence of two different Burgers vectors so that either a net bias was developed between the two components, or, as one of the components was sessile, point defect absorption would be limited. The present results indicate that either the Burgers vector distribution has little effect on swelling, or the magnitude of swelling is independent of differences in dislocation response in isolated regions.

Two instances were found where either heat-to-heat variations or heat treatment variations led to differences in density change. It is possible to provide an explanation for both situations. In the case of MA957, swelling was generally restricted to large recrystallized regions. Therefore, it is likely that the differences in density change in the two batches of MA957 were a result of different volume fractions of recrystallized regions, with batch T88793 containing more recrystallization. No attempt has been made to verify this. However, the differences in HT-9 are due to heat treatment, such that the lower tempering temperature resulted in lower swelling. Lower tempering temperatures result in finer distributions of carbide precipitation and less complete relaxation of the dislocation structures generated from the Martensite transformation. Both of these differences can be expected to delay the onset of swelling. Also, precipitation will be less complete at the lower tempering temperature so that during subsequent irradiation, further precipitation can occur that would create densification, offsetting the swelling due to void growth and producing a lower total density change measurement. The lower swelling found in HT-9 following the lower tempering temperature is likely a combination of these factors.

## CONCLUSIONS

Alloys HT-9 in two heat treatment conditions, T9, MA956, and two experimental batches of MA957 have been irradiated in the FFTF/MOTA at 420°C to 200 dpa and then measured for density change and examined by transmission electron microscopy. All alloys are found to be highly radiation resistant.

1. Swelling as measured by density change was less than 2%.

2. All specimens contained cavities, but in the ODS alloys, large regions were found with negligible cavitation, probably a remnant from mechanical alloying. Voids in the Martensitic steels were non-uniformly distributed within laths. Recrystallized regions, manufacturing defects in the MA957 specimens, contained the greatest swelling.

3. Dislocation evolution included both $\frac{a}{2}$<111> and a<100> Burgers vectors, and similar swelling response was found in regions with different Burgers vector distributions.

4. Voids were generally truncated between dodecahedra and cubes. Some variation in shape was found as a function of size.

5. Variations in swelling were found from heat-to-heat variation in MA957 and from heat treatment variation in HT-9.

6. Microstructural changes from irradiation to high dose are not expected to significantly change mechanical properties. The life limits are expected to arise due to embrittlement from phase separation ($\alpha'$) and intermetallic phase precipitation (chi and Laves) governed to some extent by the transmutation of iron to manganese.

## FUTURE WORK

This work is a continuing effort.

REFERENCES

1. A. N. Niemi, M. G. McKimpson and D. S. Gelles, "Processing of Two Iron-Chromium Oxide Dispersion Strengthened Steels by Mechanical Alloying," DOE/ER-0313/6 (1989) 187.

2. A. N. Niemi, M. G. McKimpson and D. S. Gelles, "Improved Processing for Two Ferritic Low Activation Oxide Dispersion Strengthened Steels" DOE/ER-0313/8, (1990) 177.

3. J. J. Fischer, US Patent 4,075,010, February 21, 1978.

4. D. S. Gelles and A. Kohyama, "Microstructural Examination of HT-9 Irradiated in the FFTF/MOTA to 110 dpa," Fusion Reactor Materials Semiannual Progress Report for the Period Ending March 31, 1989, DOE/ER-0313/6 (March 1989) 193.

5. D. S. Gelles, "Microstructural Development in Reduced Activation Ferritic Alloys Irradiated to 200 DPA at 420°C," J. Nucl. Mater., (1994), also included in DOE/ER-0313/15.

6. F. A. Garner and L. R. Greenwood, "Calculation of Displacement Levels for Pure Elements and Most Multicomponent Alloys Irradiated in FFTF MOTA-1F," Fusion Reactor Materials Semiannual Progress Report for the Period Ending March 31, 1992, DOE/ER-0313/12 (July 1992) 54.

7. D. S. Gelles and R. L. Meinecke-Ermi, "Swelling in Simple Ferritic Alloys Irradiated to High Fluence," Alloy Development for Irradiation Performance Semiannual Progress Report for the Period Ending September 30, 1983, DOE/ER-0045/11 (March 1984) 103.